Multidecadal loss of surface thermal structure in the largest marine upwelling ecosystems

Mario A. Pardo[1,*] & Emilio Beier[2]

1. Secretaría de Ciencia, Humanidades, Tecnología e Innovación (SECIHTI) – Centro de Investigación Científica y de Educación Superior de Ensenada, Baja California (CICESE) – Unidad Académica La Paz. Laboratorio de Macroecología Marina. La Paz, Baja California Sur 23050, Mexico. *Corresponding author. E-mail: mpardo@cicese.mx. ORCID: 0000-0003-1248-3399
2. CICESE – Unidad Académica La Paz, Laboratorio de Macroecología Marina. La Paz, Baja California Sur 23050, Mexico. Email: ebeier@cicese.mx. ORCID: 0000-0001-8478-7709

Abstract

Step horizontal gradients of sea surface temperature (SST) occur around upwelling cores, eddies, meanders, current boundaries, island-effect mixing areas, among many other oceanographic features. These thermally structured areas provide ideal turbulence for phytoplankton growth and biomass aggregation, triggering complex and abundant food webs, in turn exploited by populations of marine megafauna and fisheries. How the distribution and degree of this surface heterogeneity has varied at climate-change scales is unknown. In this study, we prove that the horizontal surface thermal structure of the ocean has declined steadily in the most important upwelling ecosystems during the last 41 years (1982-2022: -0.1°C of SST standard deviation within 0.25x0.25-dregree cells at the seasonal upwelling peak). Years with low thermal structure showed remaining hotspots towards upwelling cores, close to shore. The mechanisms of this long-term decline remain unclear. The correlation with the mean SST itself was negative but non-consistent among upwelling regions, while the negative correlation with the steadily increasing absolute dynamic topography was strong in all regions. This points to a multidecadal heat content gain along the water column as a potential cause of the homogenization process. Arguably, this loss in sea surface thermal structure could be related to described declines and redistributions of some marine megafauna species.

Keywords

Climate change, ocean warming, sea surface heterogeneity, SST spatial standard deviation, absolute dynamic topography.

Significance Statement

The steady negative trend of sea surface thermal structure discovered in this study would imply a reduction of areas for biomass retention, and the aggregation of prey and predators in upwelling ecosystems, including species targeted by fisheries.

Introduction

Local horizontal thermal heterogeneity of the ocean's surface at local scales results from diverse forcing, mainly those producing eddy-induced thermocline shoaling [1], island-effect water-column mixing [2,3], upwelling [4–6], and convergence of currents or water masses [7]. All these processes can expose cold water from subsurface layers to the warm surface, creating horizontal step thermal gradients. Such horizontal heterogeneity is important ecologically, because it produces physical boundaries where biomass can be retained [8], but also because the turbulence in those areas is lower than that at the upwelling, mixing, or shoaling cores, which benefits phytoplankton's nutrient intake (i.e. ideal turbulence) and growth [9,10]. Thus, such areas are often used as critical feeding habitats by a large variety of predators, including protected species [11–13] and species target for fisheries [14,15].

The long-term trends of sea surface temperature in the world's largest upwelling systems have shown an increase at multi-decadal scales [16]. This has important implications for marine species distributions and abundances, such as more frequent occurrence of tropical species in temperate waters, in a process often referred to as tropicalization [17,18]. The number and persistence of major current-boundary fronts has also increased in the last 40 years at large spatial scales, although the mechanisms are not clear [19]. Nevertheless, it is unknown whether the level of surface thermal structure at small spatial scales has suffered a similar trend.

Our objective was to estimate the long-term trend of the sea surface thermal structure within the four major upwelling systems of the world (Fig. 1). Our hypothesis was that the known rising temperatures of the ocean would produce a progressive homogenization of the surface and therefore a negative trend of the local horizontal thermal structure. For that, we studied the standard deviations of sea surface temperature (SSD_{SST}) within 0.25x0.25-degree cells, both spatially and temporally. To understand the physical context of these changes, we also analyzed the sea surface temperature (SST) and the absolute dynamic topography (ADT), at the same resolution.

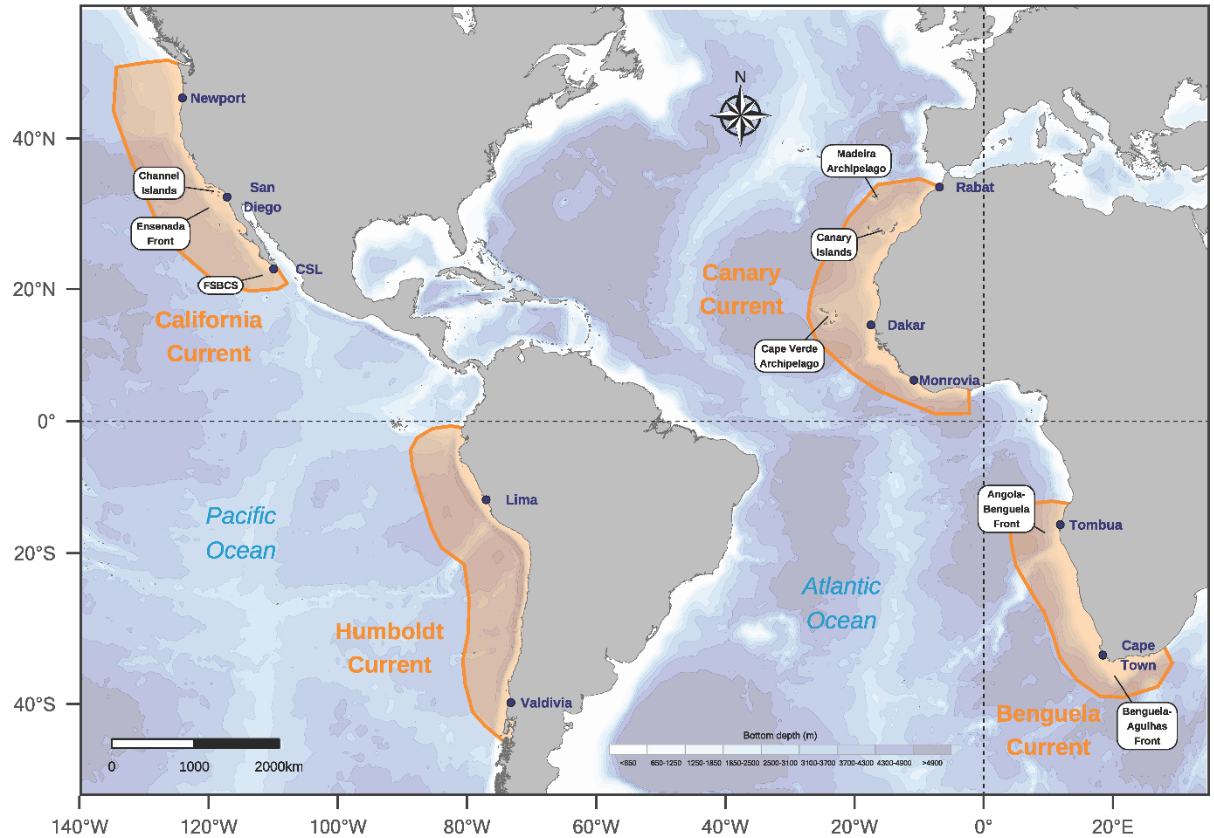

Figure 1. The largest marine upwelling ecosystems (orange polygons), with some coastal cities' locations for reference, and the oceanographical and morphological features mentioned in the manuscript. The map was created with R's package "ggplot2" (https://ggplot2.tidyverse.org/), using coastlines from the Global Self-consistent, Hierarchical, High-resolution Geography Database (http://www.soest.hawaii.edu/pwessel/gshhg/) and the topography from Scripps Institution of Oceanography's Satellite Geodesy (https://topex.ucsd.edu/marine_topo/).

Methods

We based all our data processing and analysis on two freely available products of satellite-measured environmental variables: the sea surface temperature (SST; [20] and the absolute dynamic topography of the ocean's surface (ADT; [21–23]; delimited geographically by polygons representing the areas of influence of the four largest upwelling ecosystems of the world (Fig. 1; [24,25]. SST was used to obtain the spatial standard deviations of the variable (SST_{SSD}) within 0.25x0.25-degree cells, as a quantitative index of local surface thermal structure, which was the main concern of the study, as well as to explore the correlation between the temporal trend of both variables. The ADT was also used to understand possible correlation with the SST_{SSD}, because it indicates heat gain along the water column, increasing the total volume and therefore the surface height respect to a geoid of reference [26].

SST data came from the National Oceanic and Atmospheric Administration's Advanced Very-High-Resolution Radiometer (AVHRR) Pathfinder Program (Version 5.3; https://www.ncei.noaa.gov/products/avhrr-pathfinder-sst; [20]. The original dataset consisted of daily horizontal layers of 0.05-degree cells. Only nighttime values were used, and all values catalogued by Pathfinder as inferior to "best quality" were discarded.

We decided to identify areas with high horizontal SST variability (i.e. sea surface thermal structure) by estimating the standard deviation of the variable in cells of 0.25-degree resolution (~25km^2). This means that each estimation would come from ~25 values of the original resolution of SST (0.05-degree cells). Let $T_{i,j}$ represent an SST value at the original resolution of 0.05 degrees, where i and j are indices for latitude and longitude, respectively. Now, let $\sigma_{x,y}$ represent the standard deviation of SST in a new cell from a new lower resolution of 0.25 degrees, where x and y are latitude and longitude indices for that coarser grid. Then, the standard deviation of SST at a 0.25-degree resolution would be (Eq. 1):

$$\sigma_{x,y} = \sqrt{\frac{1}{N}\sum_{i=1}^{n}\sum_{j=1}^{m}\left(T_{i,j} - \mu_{x,y}\right)^2} \qquad [1]$$

Where N is the total number of 0.05-degree resolution cells with valid values, $T_{i,j}$ are the SST values within the 0.25-degree resolution cell, and $\mu_{x,y}$ is the mean SST value within the 0.25-degree resolution cell, calculated as (Eq. 2):

$$\mu_{x,y} = \frac{1}{N}\sum_{i=1}^{n}\sum_{j=1}^{m}T_{i,j} \qquad [2]$$

We argue this standard deviation is a good representation of the horizontal thermal heterogeneity at small spatial scales, where high values indicate a more structured surface and therefore horizontal boundaries. We called this variable spatial standard deviation of SST (SST_{SSD}), and it was the main concern of this study. SST_{SSD} values were discarded if they came from less than three SST values at the original resolution. The ADT data came from the Copernicus Marine Service (https://marine.copernicus.eu/) at an original daily 0.25-degree resolution, matching the new resolutions of SST and SST_{SSD}. This scale was important, because mean values for larger areas would mask some mesoscale features (i.e. the first baroclinic mode), whereas smaller areas could include some sub-mesoscale phenomena [27,28].

To better understand the spatio-temporal patterns of SST_{SSD}, and underlaying mechanisms, we reproduced all its processing and analyses on the SST and ADT. Since our main interest was the long-term trend of the variables, we discarded the seasonal variability. For that, we chose as representative season the upwelling peak period for each ecosystem and discarded data of the rest of the year. The number of days for averaging the variable each year aimed to maximize the time-series' cell sample size for each year. We tested with periods of one day, 15 days, one month, and three months. We finally kept the latter given its acceptable number of cells with available values of SST and SST_{SSD} (Supplementary Material Fig. S1). Therefore, the periods averaged for all variables were May to July for the California Current [29] and the Canary Current [30], and October to December for the Humboldt Current [31] and the Benguela Current [32].

The first step was comparing the three variables spatially during the same year. For this, we mapped the values of the last year of the series (2022) for each upwelling. Then, we produced annual maps of SST_{SSD} for the entire time series to inspect potential redistribution of highly structured areas in each upwelling ecosystem. The long-term trend of each variable throughout the 41-year time series was defined as the slope of a simple linear regression of the variable means within the upwelling ecosystem polygon as a function of time in years. The regressions were independent for each variable and each upwelling ecosystem. The estimation of the slopes posterior distributions and time series predictions were made in a Bayesian fixed-effects regression analysis, using the integrated nested Laplace approximation (INLA) [33]. After an initial inspection of the three variables, we decided to assume a Gaussian likelihood with default uninformative priors. From the values of the slopes' posterior distributions, we estimated the probability of them being larger or lower than zero and extracted the quantiles of the median and those delimiting the range of the 95%-credible interval. The medians of the annual predictions were used to estimate an approximate Bayesian R-squared [34], which represents the proportion of the total variability explained by the long-term trend and is an indicator of model's accuracy.

Finally, we explored the correlation between the SST_{SSD} with the SST and the ADT at each upwelling ecosystem. We used the same modeling strategy of the variables' time series described above. In this case, extreme values of the probability of the slope being positive or negative would indicate a strong correlation, whereas values close to 0.5 would indicate null correlation [35].

All data reading, processing, analyses, and representation were coded in R [36], using the packages: "dplyr" [37], "ggplot2" [38], "ggsn" [39], "INLA" [33], "maptools" [40], "Matrix" [41], "ncdf4" [42], "PBSmapping" [43], "plyr" [44], "showtext" [45], "sp" [46], "sysfonts" [47], and "viridisLite" [48].

Results

Spatiality

The general distribution patterns of the spatial standard deviation of sea surface temperature (SST_{SSD}), as index of sea surface thermal structure (*i.e.* heterogeneity), showed persistent high values close to known coastal upwelling cores and meanders, frontal systems, coastal trapped waves, and island-effect regions, among others (Fig. 2A and Supplementary Material Fig. S1). This confirmed the variable as an indicator of the main sources of thermal heterogeneity in the ocean's surface. By comparing the maps of SST_{SSD} with those of sea surface temperature (SST) and absolute dynamic topography (ADT) (Fig. 2), it was evident that the former's highest values were produced by diverse oceanographic conditions:

The distribution of SST showed a latitudinal gradient from warmer waters towards the Equator to colder waters farther from it, except for the coastal upwelling cores, which exhibited very cold waters in mid-latitude coastal regions. The Benguela Current was the only one whose upwelling cold core was bounded by warm waters both to the south and to the north (Fig. 2B). The SST_{SSD} was also very high around the upwelling cores, projecting to more oceanic waters in meander-like shapes. This was more evident in the California and Canary currents, where these features extended far from the coast. Nevertheless, the regions with high SST_{SSD} were not only those influenced by coastal upwelling. Low values of ADT in regions far from the coastal upwelling cores indicated other phenomena shoaling the thermocline or producing mixing. For example, in the California Current, west off Cabo San Lucas, low values of ADT occurred (CSL in Fig. 2C), as well as high SST_{SSD} values (Fig. 2A), apparently independent from the main upwelling core. Likewise, in the Benguela Current, very low values of ADT occurred southwest of the main upwelling cold core (Fig. 2C), limiting with a very warm surface tongue extending longitudinally southeast off Cape Town (Fig. 2B), which was visible as a region with very high values of SST_{SSD} (Fig. 2A). Around some archipelagos, the SST_{SSD} high values seemed to capture island-effect phenomena (Fig. 2A and Supplementary Material Figs. S2 and S3), for example, in the Channel Islands (CHI), the Canary Islands, and Cape Verde Archipelago. Other known oceanographic features observable from the distribution of SST_{SSD} were the Ensenada Front (EF) and the Frontal System off Baja California Sur (FSBCS), the Angola-Benguela Front (ABF), and the Benguela-Agulhas Front (BAF) (Figs. 1 and 2).

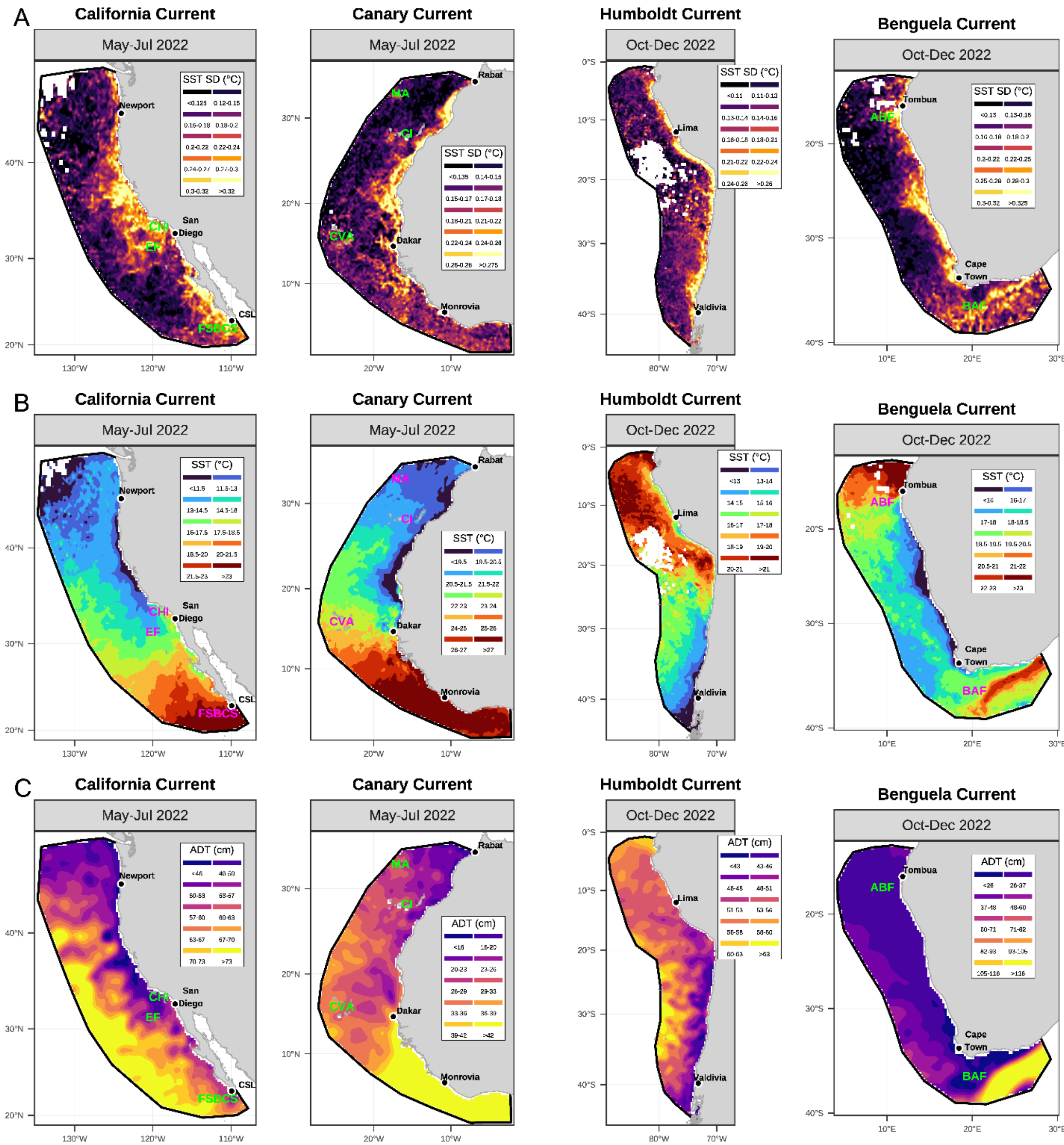

Figure 2. Spatial distribution of the sea surface variables analyzed for the three-month period of upwelling peak at each of the four main upwelling ecosystems during the year 2022: A) The sea surface temperature spatial standard deviation (SST SD), B) the SST, and C) the absolute dynamic topography (ADT). Labels show the abbreviations of some oceanographic features described in the literature for each upwelling ecosystem (portrayed in Fig. 1).

Multidecadal trends

The 41-year time series analysis of mean SST_{SSD} resulted in negative long-term trends for all the upwelling systems (Fig. 3A). All slopes were lower than zero with a probability of 1. The California Current had the most pronounced decrease in SST_{SSD}, with an slope of -0.05°C in 41 years (95%-CI: -0.063:-0.034) whereas the lesser decrease was that of the Humboldt Current, with -0.029°C (95%-CI: -0.046:-0.013). Although the negative trends were evident, the variability of the observations was high, since the long-term trend only accounted for 48% of the total variance for the California Current, 35% for the Canary Current, 24% for the Humboldt Current, and 30% for the Benguela Current (Bayesian R-squared values; Fig. 3A), which implies high shorter-term (i.e. interannual) variability. Contrary to the other two surface variables, the SST_{SSD} showed a very similar scale of values among upwelling systems, as well as more similar interannual variability (Fig. 3).

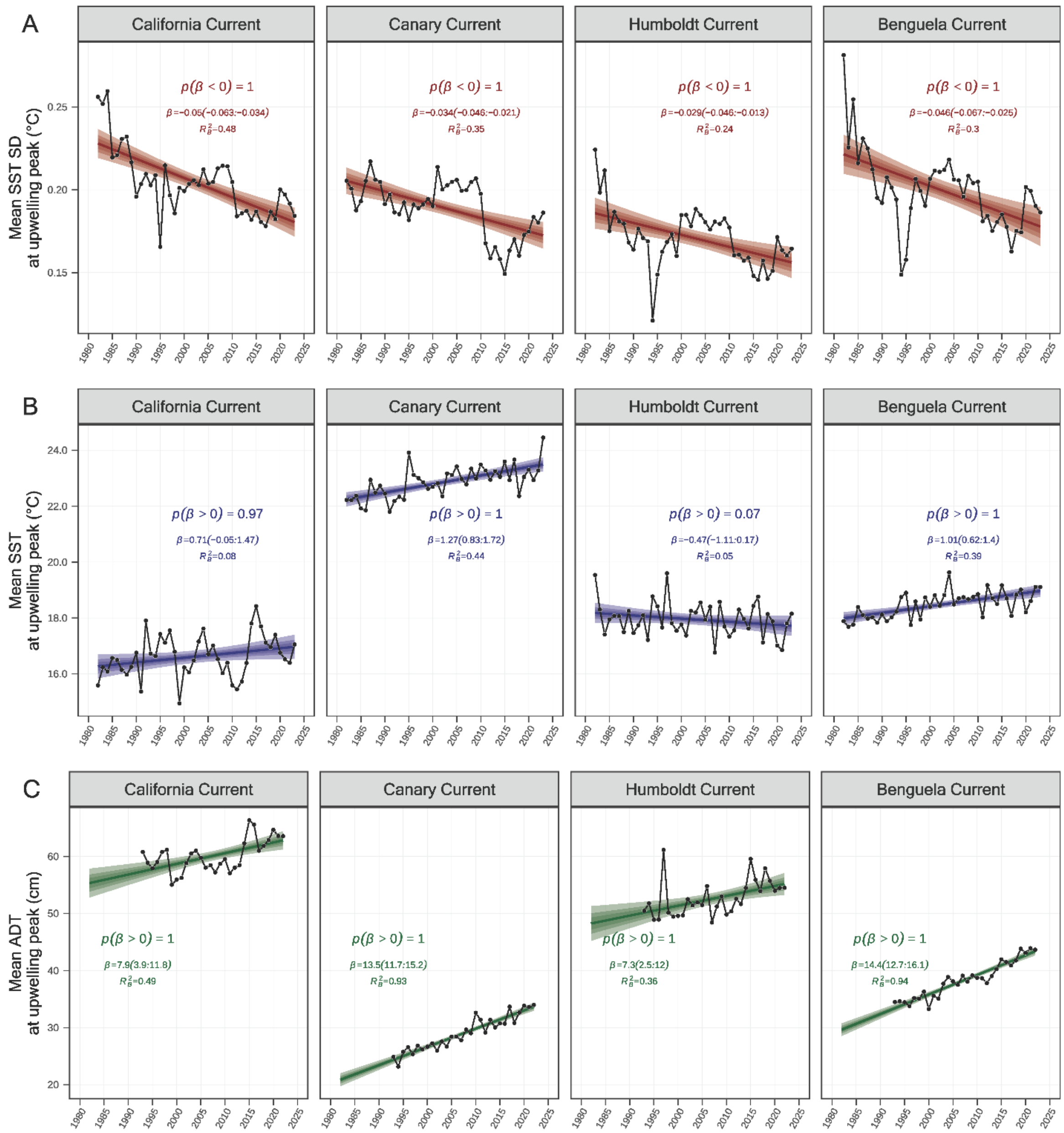

Figure 3. Long-term linear trends of A) the mean spatial standard deviation (SD) of sea surface temperature (SST), B) the SST, and C) the absolute dynamic topography of the ocean's surface (ADT), during the three-month upwelling peak for each ecosystem. Text labels within plots show the probability that the slope (β) is positive (first row), along with the 95%-credible interval of the posterior probability distribution of β (second row), and the Bayesian R-squared ($R_B{}^2$), as the proportion of the observations' variance explained by that of the median linear trend's predictions (third row).

Mean SSTs showed mostly positive long-term trends, except for the Humboldt Current (Fig. 3B). The Canary Current showed the steepest warming, with 1.27 °C in 42 years (95%-CI: 0.83:1.72), followed by the Benguela Current, with a 41-year increase of 1.01°C (955-CI: 0.62:1.44), both with a probability of positive slope of 100%. The California Current's surface warmed up 0.71 °C in 42 years (95%-CI: -0.05:1.47), with a probability of a positive slope of 97%, and the Humboldt Current presented a mostly negative trend of -0.47 °C in 42 years (95%-CI: -1.11:0.17) and a probability of positive slope of only 7% (i.e. 93%-probability of being negative). The explained variance of these long-term trends was low in general, although variable. It was 44% for the Canary Current and 39% for the Benguela Current, but only 8% and 5% for the California Current and the Humboldt Current, respectively, which indicates a much higher shorter-term variability in the latter two upwelling systems.

The long-term trends of ADT were all positive with a probability of 100%. The Benguela Current showed the steepest increase, with 14.4 cm in 42 years (95%-CI: 12.7:16.1), while the least pronounced was that of the Humboldt Current, with 7.3 cm in 42 years (95%-CI: 2.5:12) (Fig. 3C). The Bayesian R-squared values indicated that the linear long-term trend is the main source of variation of ADT in the Canary Current and the Benguela Current, with 93% and 94% of explained variance, respectively, whereas the shorter-term variability were more important in the California Current and the Humboldt Current, whose long-term trend explained only the 49% and the 36% of the total variance (Fig. 3C).

The annual maps for the complete time series of SST_{SSD} show the magnitude of the loss in surface thermal structure from the first to the last years of the series, and especially, which areas were most affected by it (Supplementary Material Figs. S2 to S5). Overall, years with low structure showed the oceanic areas as those more affected, since high values of SST_{SSD} retracted to coastal areas, close to the main upwelling cores. This was especially evident in the Canary Current, whose oceanic values dropped dramatically in years with low mean structure, while remaining high only along a narrow strip close to shore (Supplementary Material Fig. S3). This suggests a reduction in the areas with the occurrence of these structures.

Variable correlations

The regression slopes of SST_{SSD} as function of SST were mostly negative, except for that of the Humboldt Current, which was neutral (Fig. 4A). This relation could explain at most 15% of the total variance in the California Current, indicating very high dispersion. The relation with the ADT was also negative, in this case, for all upwelling systems (Fig. 4B), and was able to explain up to 22% of total variance for the Canary Current.

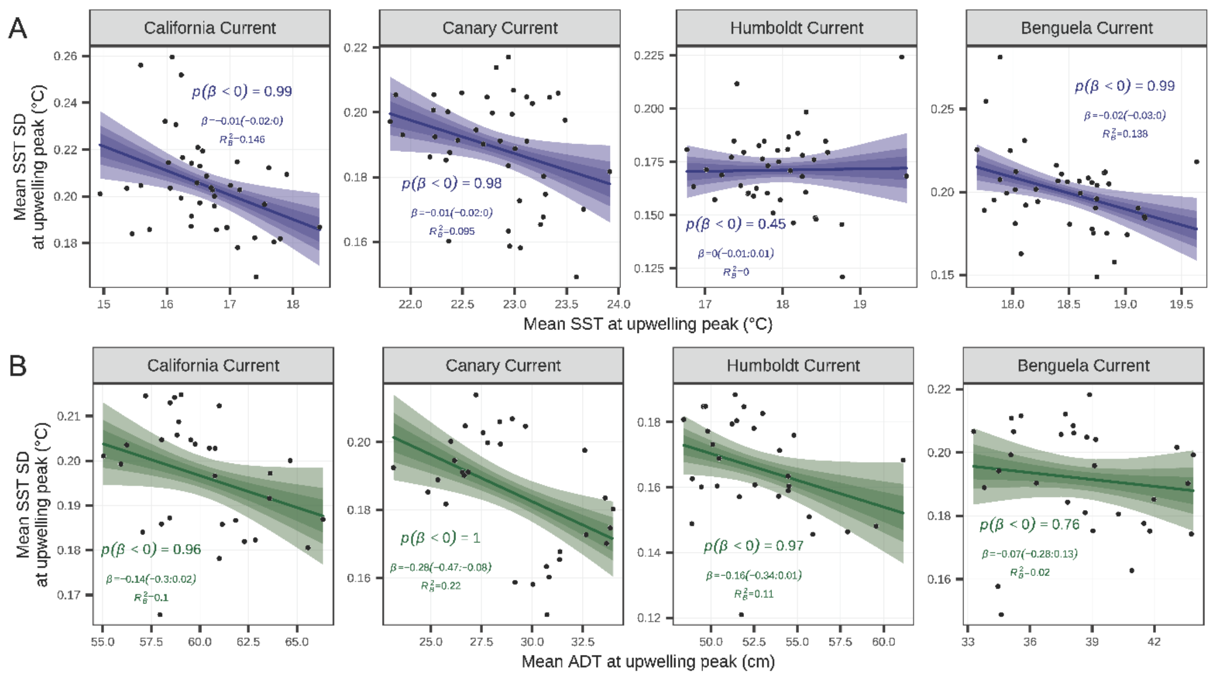

Figure 4. Correlation regressions of the mean spatial standard deviation (SD) of sea surface temperature (SST) as function of A) mean SST and B) mean absolute dynamic topography of the ocean's surface (ADT), during a three-month yearly upwelling peak at each ecosystem. Text labels within plots show the probability that the slope (β) is negative (first row), the 95%-credible interval of the posterior probability distribution of β (second row), and the Bayesian R-squared ($R_B{}^2$), as the proportion of the observations' variance explained by that of the median linear trend's predictions (third row).

Discussion

The mean values of SST_{SSD} observed in this study ranged from 0.005 to 2.6 °C, which agree with the typical horizontal variability of the ocean's SST previously reported for the spatial resolution studied (~25 km^{-2}) [27]. Similar variability has been observed in studies of various oceanographic features, including upwelling cores [4–6], eddy-like circulation [1], and current-boundary fronts [7]. It is then very important to limit the interpretation of the patterns described in this study to such specific spatial resolution, because at larger scales, the SST_{SSD}'s could be much higher and influenced by other oceanographic dynamics, not targeted by this study. Such spatial scale would explain the very similar values of SST_{SSD} and their long-term trends among all upwelling ecosystems (Fig. 3A), in contrast to those of SST and ADT, which showed very high variability (Figs. 2A and 2B). We think this is precisely the reason our results seem to differ drastically from those recently published in Nature Communications [19] on the evolution of persistent fronts in the large marine ecosystems, for the same 40-year period of our study. Those results describe a positive trend on the number and intensity of such fronts, contrary to the negative trends of the sea surface thermal structure described here. We think this discrepancy is due to the very different spatial resolutions studied. Whereas Xing et al. focused their analysis at a resolution of 100 km, we based our analyses in 25-km^{-2} areas, a much finer resolution. Another important aspect that would help to explain the completely different trends: Xing et al.'s study managed to detect only gradients perpendicular to the coast and only in relatively coastal areas. Since the direction of those fronts makes them aligned latitudinally, it would be possible that latitudinal gradients in temperature along the coast and at large scales have increased due to a tropicalization process, in which warmer waters reach higher latitudes progressively. Nevertheless, more studies are needed on the dynamics of surface thermal structures at different scales and detected by different methods.

The highest values of SST_{SSD} indicated consistently the influence of oceanographic phenomena of different nature (e.g. upwelling cores, current boundaries, island effect, and regional fronts) (Fig. 2A). This is because this variable incorporates only the local scale of spatial variation, whereas SST and ADT include processes responding to global variability. The step decrease in yearly mean SSD_{SST}'s was manifest and consistent in all upwelling systems (Fig. 3A), and it implied a reduction in surface thermal structure, both in terms of its area coverage and its magnitude (Supplementary Material Figs. S2 to S5). However, the potential causes of this phenomenon are unclear. In this study, we inspected other two physical variables to try to understand better the environmental context under which the SSD_{SST} multidecadal decrease occurred: the SST and ADT. From them, the ADT showed a consistent increase in all upwelling systems (Fig. 3C). Since high ADT values would reflect a heat gain along the water column [23,49], one could argue that it would produce a progressive thermal homogenization of the sea surface, as has been suggested in model projections of the upwelling system dynamics [50]. The strong correlation between ATD and SSD_{SST} supports this possibility (Fig. 4B).

The SST's long-term trend was also positive among upwelling systems, except for the Humboldt Current System, whose slope was almost certainly negative (Fig. 3B). This contradicts what was shown by that of the ADT, which was certainly positive (Fig. 3C), because if the water column suffered enough heat gain to produce an increase of ADT, one would expect that such gain would be also shown by the temperature at surface. Solving this problem is beyond the scope of this study, but it is possible that the close influence of the Antarctic Circumpolar Current on this upwelling system [51,52], which would maintain its surface colder than the others', which are farther from the poles.

According to the Bayesian R-squared values, it was clear that the California Current and the Humboldt Current systems exhibited higher variability in SST and ADT respect to their linear trends than those shown by the Canary Current and the Benguela Current systems (Figs. 3B and 3C). This is likely due to the interannual occurrence of El Niño/La Niña Southern Oscillation (ENSO[53,54], which affects mainly coastal waters of the Pacific coasts of the American continent, from the Equator and frequently extending to both upwelling system cores [55]. In fact, some of the most extreme deviations from the linear trends of both variables coincided with well-known El Niño or La Niña events (e.g. 1997-1998 EL Niño, 1999 La Niña, 2011 La Niña), as well as the positive anomalies of 2014 and 2015, attributed to the northeast Pacific Marine Heat Wave [56] and the 2015 El Niño [57]. Interestingly, these anomalies do not seem to coincide at all with those exhibited by the SSD_{SST}, which were similar among the four upwelling systems. The process driving such seemingly common variability is still unknown and could be the focus of future studies.

Based on the strong relation between feeding habitats for marine megafauna and horizontal sea surface thermal structures (e.g. [11–13], as well as their importance for some fisheries, the step decreases in SSD_{SST} reported for all major upwelling systems would represent a progressive loss in critical habitat coverage with in those large marine ecosystems. Therefore, we recommend including this variable and its spatial and temporal trends as potential covariates in future habitat-based models of distribution and population trends of pelagic species. Further studies should also address the implications of this seemingly global change in surface thermal structure for marine ecosystems.

Acknowledgments

We acknowledge the hard work of NOAA's and the Copernicus Program's personnel, which made freely available the datasets used in this study.

Availability Statement

SST data can be downloaded directly from NOAA's site: https://www.ncei.noaa.gov/data/oceans/pathfinder/Version5.3/L3C/, or via any File Transfer Protocol client software. ADT data can be freely obtained following the instructions at the Copernicus site: https://help.marine.copernicus.eu/en/articles/8612591-switching-from-current-to-new-services#h_7a28461000.

Author Contributions

M.A.P.: Conceptualization, methodology, formal analysis, visualization, writing original draft, review, and editing.

E.B.: Conceptualization, review, and editing.

Funding

M.A. Pardo was funded by CICESE (Internal Project No. 691-113; P.I.: M.A. Pardo). E. Beier was funded by CICESE (Internal Project No. 691-102 P.I.: E. Beier).

Conflicts of Interests

The authors declare they do not have any known competing financial or personal interests that could influence the work presented in this article.

References

Bachman, S.D., Taylor, J.R., Adams, K.A., Hosegood, P.J., 2017. Mesoscale and Submesoscale Effects on Mixed Layer Depth in the Southern Ocean. Journal of Physical Oceanography 47, 2173–2188. https://doi.org/10.1175/JPO-D-17-0034.1

Bakun, A., 1990. Global Climate Change and Intensification of Coastal Ocean Upwelling. Science 247, 198–201. https://doi.org/10.1126/science.247.4939.198

Barker, P.F., Filippelli, G.M., Florindo, F., Martin, E.E., Scher, H.D., 2007. Onset and role of the Antarctic Circumpolar Current. Deep Sea Research Part II: Topical Studies in Oceanography 54, 2388–2398. https://doi.org/10.1016/j.dsr2.2007.07.028

Bates, D., Maechler, M., Jagan, M., 2024. Matrix: Sparse and Dense Matrix Classes and Methods.

Bivand, R., Lewin-Koh, N., 2023. maptools: Tools for Handling Spatial Objects.

Bjerknes, J., 1969. ATMOSPHERIC TELECONNECTIONS FROM THE EQUATORIAL PACIFIC 1. Monthly Weather Review 97, 163–172. https://doi.org/10.1175/1520-0493(1969)097<0163:ATFTEP>2.3.CO;2

Bost, C.A., Cotté, C., Bailleul, F., Cherel, Y., Charrassin, J.B., Guinet, C., Ainley, D.G., Weimerskirch, H., 2009. The importance of oceanographic fronts to marine birds and mammals of the southern oceans. Journal of Marine Systems 78, 363–376. https://doi.org/10.1016/j.jmarsys.2008.11.022

Casey, K.S., Brandon, T.B., Cornillon, P., Evans, R., 2010. The Past, Present, and Future of the AVHRR Pathfinder SST Program, in: Barale, V., Gower, J.F.R., Alberotanza, L. (Eds.), Oceanography from Space: Revisited. Springer Science+Business Media B.V., pp. 273–287.

Chao, S., 1987. Wind-driven motion near inner shelf fronts. J. Geophys. Res. 92, 3849–3860. https://doi.org/10.1029/JC092iC04p03849

Chavez, F.P., Bertrand, A., Guevara-Carrasco, R., Soler, P., Csirke, J., 2008. The northern Humboldt Current System: Brief history, present status and a view towards the future. Progress in Oceanography 79, 95–105. https://doi.org/10.1016/j.pocean.2008.10.012

Checkley, D.M., Barth, J.A., 2009. Patterns and processes in the California Current System. Progress in Oceanography 83, 49–64. https://doi.org/10.1016/j.pocean.2009.07.028

Chelton, D.B., Schlax, M.G., Samelson, R.M., 2011. Global observations of nonlinear mesoscale eddies. Progress in Oceanography 91, 167–216. https://doi.org/10.1016/j.pocean.2011.01.002

Di Lorenzo, E., Mantua, N., 2016. Multi-year persistence of the 2014/15 North Pacific marine heatwave. Nature Climate Change 6, 1042–1047. https://doi.org/10.1038/nclimate3082

Ducet, N., Le Traon, P.Y., Reverdin, G., 2000. Global high-resolution mapping of ocean circulation from TOPEX/Poseidon and ERS-1 and -2. J. Geophys. Res. 105, 19477–19498. https://doi.org/10.1029/2000JC900063

Ebert, U., 2001. Critical Conditions for Phytoplankton Blooms. Bulletin of Mathematical Biology 63, 1095–1124. https://doi.org/10.1006/bulm.2001.0261

Fiedler, P.C., Bernard, H.J., 1987. Tuna aggregation and feeding near fronts observed in satellite imagery. Continental Shelf Research 7, 871–881. https://doi.org/10.1016/0278-4343(87)90003-3

Garnier, S., Ross, N., Rudis, R., Camargo, A.P., Sciaini, M., Scherer, C., 2024. viridis(Lite) - Colorblind-Friendly Color Maps for R.

Garrett, C.J.R., Loder, J.W., 1981. Dynamical aspects of shallow sea fronts. Phil. Trans. R. Soc. Lond. A 302, 563–581. https://doi.org/10.1098/rsta.1981.0183

Garzoli, S.L., Gordon, A.L., 1996. Origins and variability of the Benguela Current. J. Geophys. Res. 101, 897–906. https://doi.org/10.1029/95JC03221

Gelman, A., Carlin, J.B., Stern, H.S., Dunson, D.B., Vehtari, A., Rubin, D.B., 2014. Bayesian Data Analysis, Third Edition. ed, Texts in Statistical Science. Chapman & Hall/CRC, Boca Raton, Florida, USA.

Gelman, A., Goodrich, B., Gabry, J., Vehtari, A., 2019. R-squared for Bayesian Regression Models. The American Statistician 73, 307–309. https://doi.org/10.1080/00031305.2018.1549100

Ghosal, S., Mandre, S., 2003. A simple model illustrating the role of turbulence on phytoplankton blooms. Journal of Mathematical Biology 46, 333–346. https://doi.org/10.1007/s00285-002-0184-4

Gutierrez-Guerra, M.A., Perez-Hernandez, M.D., Velez-Belchi, P., 2024. Intensified upwelling: normalized sea surface temperature trends expose climate change in coastal areas. https://doi.org/10.5194/egusphere-2024-389

Hazen, E., Friedlaender, A., Thompson, M., Ware, C., Weinrich, M., Halpin, P., Wiley, D., 2009. Fine-scale prey aggregations and foraging ecology of humpback whales Megaptera novaeangliae. Marine Ecology Progress Series 395, 75–89. https://doi.org/10.3354/meps08108

Hoolihan, J.P., Wells, R.J.D., Luo, J., Falterman, B., Prince, E.D., Rooker, J.R., 2014. Vertical and Horizontal Movements of Yellowfin Tuna in the Gulf of Mexico. Marine and Coastal Fisheries 6, 211–222. https://doi.org/10.1080/19425120.2014.935900

Huyer, A., 1983. Coastal upwelling in the California current system. Progress in Oceanography 12, 259–284. https://doi.org/10.1016/0079-6611(83)90010-1

Jacox, M.G., Hazen, E.L., Zaba, K.D., Rudnick, D.L., Edwards, C.A., Moore, A.M., Bograd, S.J., 2016. Impacts of the 2015-2016 El Niño on the California Current System: Early assessment and comparison to past events: 2015-2016 El Niño Impact in the CCS. Geophysical Research Letters 43, 7072–7080. https://doi.org/10.1002/2016GL069716

Kessler, W.S., 2006. The circulation of the eastern tropical Pacific: A review. Progress in Oceanography 69, 181–217. https://doi.org/10.1016/j.pocean.2006.03.009

Le Fèvre, J., 1986. Aspects of the Biology of Frontal Systems. Advances in Marine Biology 23, 163–299.

Le Traon, P.Y., Nadal, F., Ducet, N., 1998. An Improved Mapping Method of Multisatellite Altimeter Data. J. Atmos. Oceanic Technol. 15, 522–534. https://doi.org/10.1175/1520-0426(1998)015<0522:AIMMOM>2.0.CO;2

Lynn, R.J., 2003. Seasonal renewal of the California Current: The spring transition off California. Journal of Geophysical Research 108. https://doi.org/10.1029/2003JC001787

Mason, E., Colas, F., Molemaker, J., Shchepetkin, A.F., Troupin, C., McWilliams, J.C., Sangrà, P., 2011. Seasonal variability of the Canary Current: A numerical study. J. Geophys. Res. 116, C06001. https://doi.org/10.1029/2010JC006665

Montecino, V., Lange, C.B., 2009. The Humboldt Current System: Ecosystem components and processes, fisheries, and sediment studies. Progress in Oceanography 83, 65–79. https://doi.org/10.1016/j.pocean.2009.07.041

Olbers, D., Willebrand, J., Eden, C., 2012. Ocean Dynamics. Springer Berlin Heidelberg, Berlin, Heidelberg. https://doi.org/10.1007/978-3-642-23450-7

Orsi, A.H., Whitworth, T., Nowlin, W.D., 1995. On the meridional extent and fronts of the Antarctic Circumpolar Current. Deep Sea Research Part I: Oceanographic Research Papers 42, 641–673. https://doi.org/10.1016/0967-0637(95)00021-W

Oyarzún, D., Brierley, C.M., 2019. The future of coastal upwelling in the Humboldt current from model projections. Clim Dyn 52, 599–615. https://doi.org/10.1007/s00382-018-4158-7

Pebesma, E., Bivand, R., 2005. Classes and methods for spatial data in R.

Philander, S.G., 1990. El Niño, La Niña, and the southern oscillation, International geophysics series. Academic Press, San Diego.

Pierce, D., 2023. ncdf4: Interface to Unidata netCDF (Version 4 or Earlier) Format Data Files.

Qiu, Y., 2023. showtext: Using Fonts More Easily in R Graphs.

Qiu, Y., 2022. sysfonts: Loading Fonts into R.

R Core Team, 2025. R: A language and environment for statistical computing, in: R Foundation for Statistical Computing. Vienna, Austria.

Rebert, J.P., Donguy, J.R., Eldin, G., Wyrtki, K., 1985. Relations between sea level, thermocline depth, heat content, and dynamic height in the tropical Pacific Ocean. Journal of Geophysical Research 90, 11719. https://doi.org/10.1029/JC090iC06p11719

Rue, H., Martino, S., Chopin, N., 2009. Approximate Bayesian inference for latent Gaussian models by using integrated nested Laplace approximations. Journal of the Royal Statistical Society. Series B (Statistical Methodology) 71, 319–392.

Santos-Baquero, O., 2019. ggsn: North Symbols and Scale Bars for Maps Created with “ggplot2” or “ggmap.” R package version 0.5.0.

Scales, K.L., Miller, P.I., Hawkes, L.A., Ingram, S.N., Sims, D.W., Votier, S.C., 2014. REVIEW: On the Front Line: frontal zones as priority at-sea conservation areas for mobile marine vertebrates. J Appl Ecol 51, 1575–1583. https://doi.org/10.1111/1365-2664.12330

Schnute, J., Boers, N., Haigh, R., 2023. PBSmapping: Mapping Fisheries Data and Spatial Analysis Tools.

Sudo, K., Maehara, S., Nakaoka, M., Fujii, M., 2022. Predicting Future Shifts in the Distribution of Tropicalization Indicator Fish that Affect Coastal Ecosystem Services of Japan. Front. Built Environ. 7, 788700. https://doi.org/10.3389/fbuil.2021.788700

Ueno, H., Bracco, A., Barth, J.A., Budyansky, M.V., Hasegawa, D., Itoh, S., Kim, S.Y., Ladd, C., Lin, X., Park, Y.-G., Prants, S., Ross, T., Rypina, I.I., Sasai, Y., Trusenkova, O.O., Ustinova, E.I., Zhong, Y., 2023. Review of oceanic mesoscale processes in the North Pacific: Physical and biogeochemical impacts. Progress in Oceanography 212, 102955. https://doi.org/10.1016/j.pocean.2022.102955

Vergés, A., Steinberg, P.D., Hay, M.E., Poore, A.G.B., Campbell, A.H., Ballesteros, E., Heck, K.L., Booth, D.J., Coleman, M.A., Feary, D.A., Figueira, W., Langlois, T., Marzinelli, E.M., Mizerek, T., Mumby, P.J., Nakamura, Y., Roughan, M., van Sebille, E., Gupta, A.S., Smale, D.A., Tomas, F., Wernberg, T., Wilson, S.K., 2014. The tropicalization of temperate marine ecosystems: climate-mediated changes in herbivory and community phase shifts. Proc. R. Soc. B. 281, 20140846. https://doi.org/10.1098/rspb.2014.0846

von Arx, W.S., 1965. Absolute dynamic topography. Limnology and Oceanography 10.

Walker, G.T., 1925. Correlation In Seasonal Variations of Weather - A Further Study Of World Weather. Mon. Wea. Rev. 53, 252–254. https://doi.org/10.1175/1520-0493(1925)53<252:CISVOW>2.0.CO;2

Wickham, H., 2016. ggplot2: Elegant graphics for data analysis, Use R! Springer.

Wickham, H., 2011. The Split-Apply-Combine Strategy for Data Analysis. Journal of Statistical Software 40, 1–29. https://doi.org/10.18637/jss.v040.i01

Wickham, H., François, R., Henry, L., Müller, K., Vaughan, D., 2023. dplyr: A Grammar of Data Manipulation. R package version 1.1.4.

Wolanski, E., Hamner, W.M., 1988. Topographically Controlled Fronts in the Ocean and Their Biological Influence. Science 241, 177–181. https://doi.org/10.1126/science.241.4862.177

Xing, Q., Yu, H., Wang, H., 2024. Global mapping and evolution of persistent fronts in Large Marine Ecosystems over the past 40 years. Nat Commun 15, 4090. https://doi.org/10.1038/s41467-024-48566-w

Supplementary Material

Multidecadal loss of surface thermal structure in the largest marine upwelling ecosystems

Mario A. Pardo[1,*] & Emilio Beier[2]

3. Secretaría de Ciencia, Humanidades, Tecnología e Innovación (SECIHTI) – Centro de Investigación Científica y de Educación Superior de Ensenada, Baja California (CICESE) – Unidad Académica La Paz. Laboratorio de Macroecología Marina. La Paz, Baja California Sur 23050, Mexico. *Corresponding author. E-mail: mpardo@cicese.mx. ORCID: 0000-0003-1248-3399
4. CICESE – Unidad Académica La Paz, Laboratorio de Macroecología Marina. La Paz, Baja California Sur 23050, Mexico. Email: ebeier@cicese.mx. ORCID: 0000-0001-8478-7709

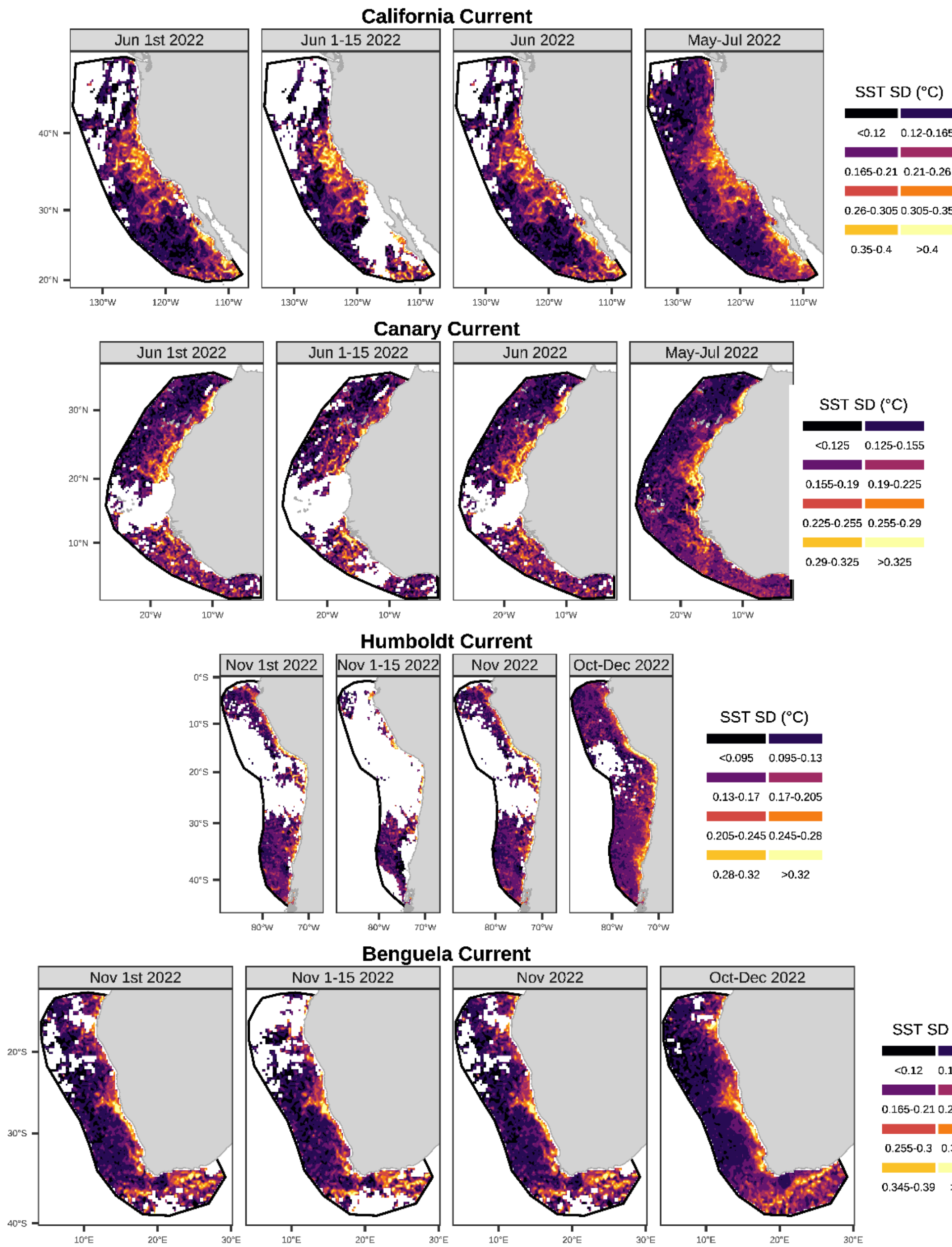

Figure S1. Example of different temporal resolutions for the standard deviation (SD) of sea surface temperature (SST). From left to right: one day, 15 days, one month, and three months. The periods were chosen based on the typical upwelling peak season at each ecosystem. Note that the three-month resolution maximizes sample size and allows for the identification of more horizontal structures.

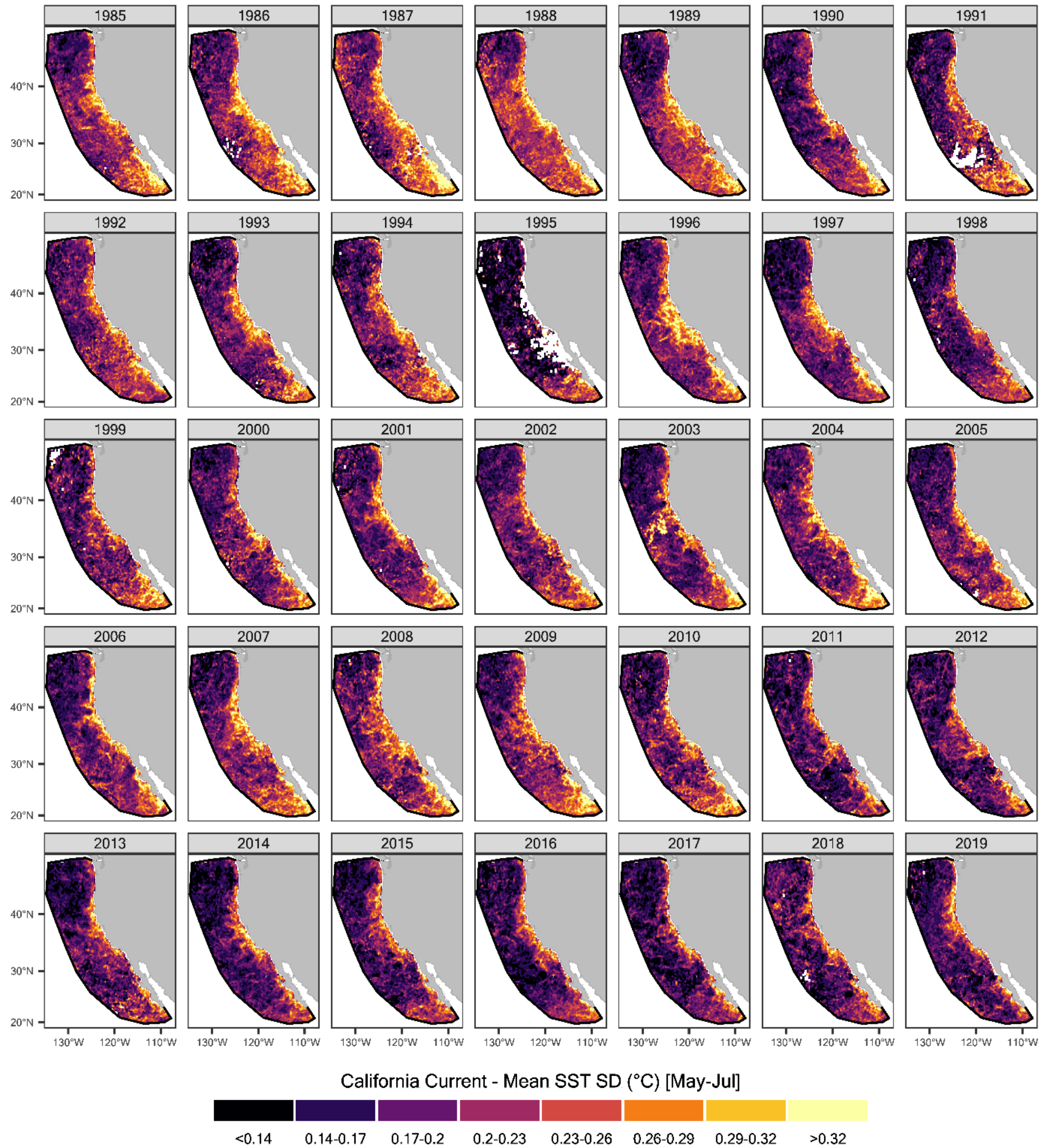

Figure S2. The three-month mean spatial standard deviation (SD) of sea surface temperature (SST) in the California Current spanning 1985-2019.

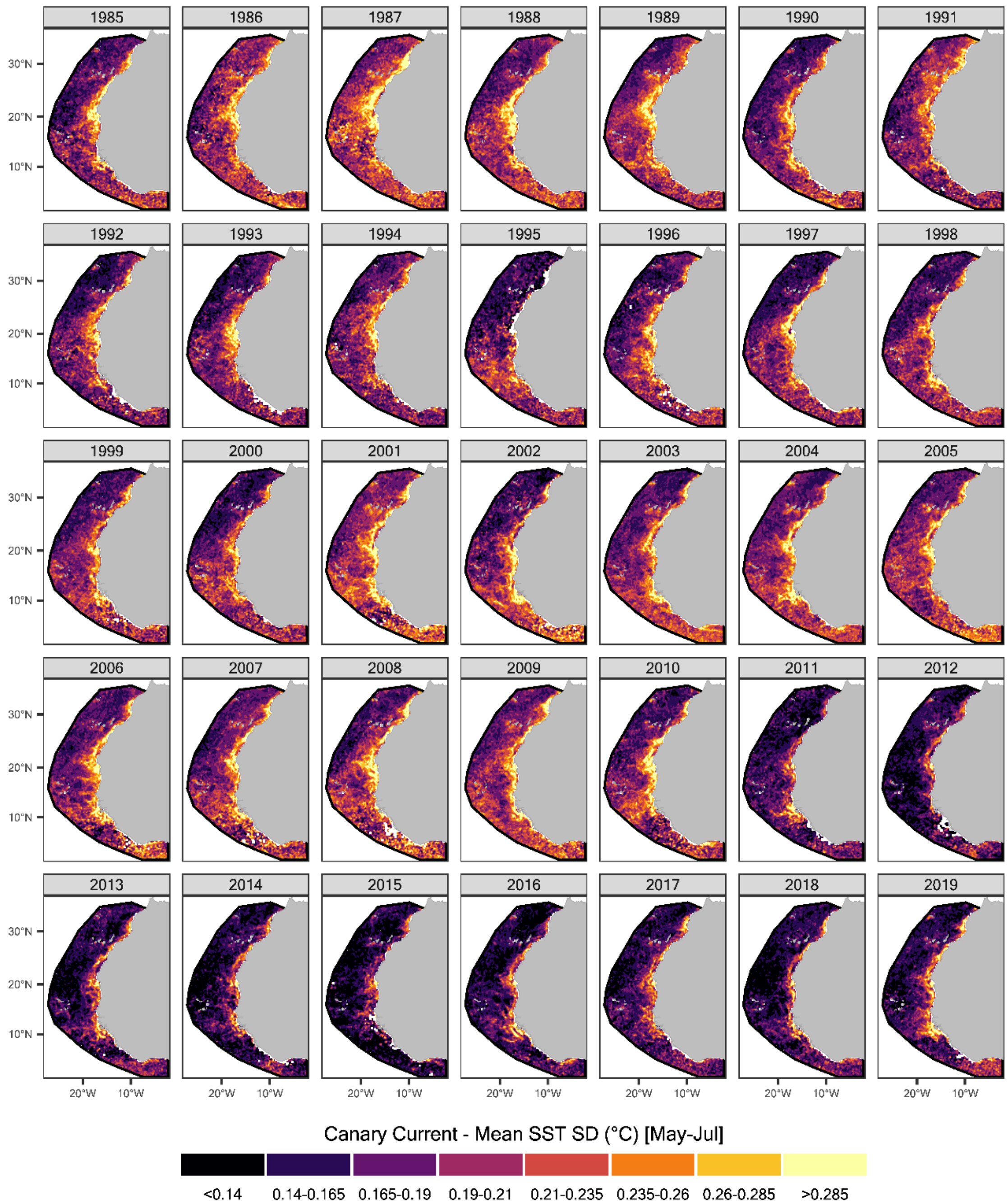

Figure S3. The three-month mean spatial standard deviation (SD) of sea surface temperature (SST) in the Canary Current spanning 1985-2019.

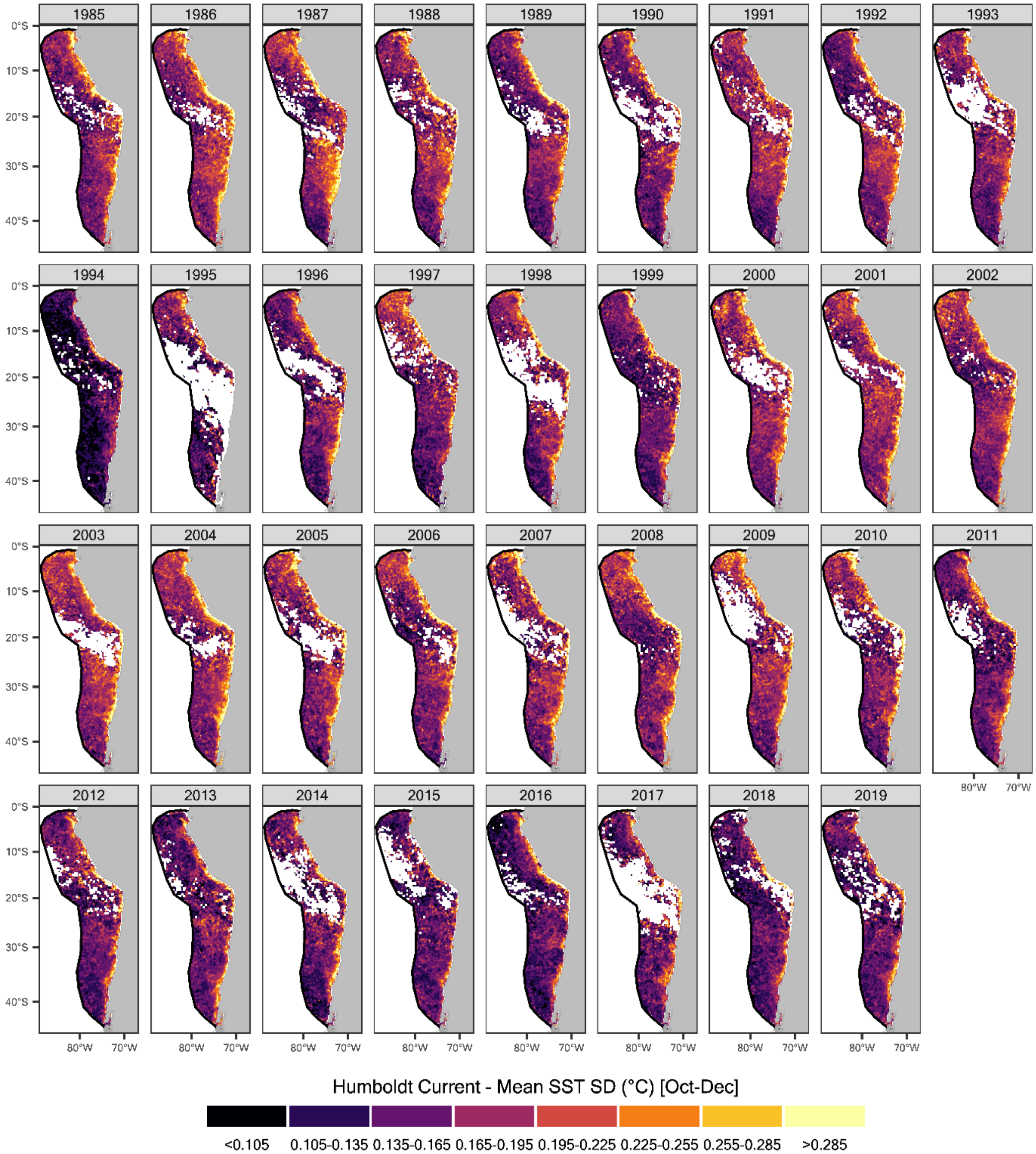

Figure S4. The three-month mean spatial standard deviation (SD) of sea surface temperature (SST) in the Humboldt Current spanning 1985-2019.

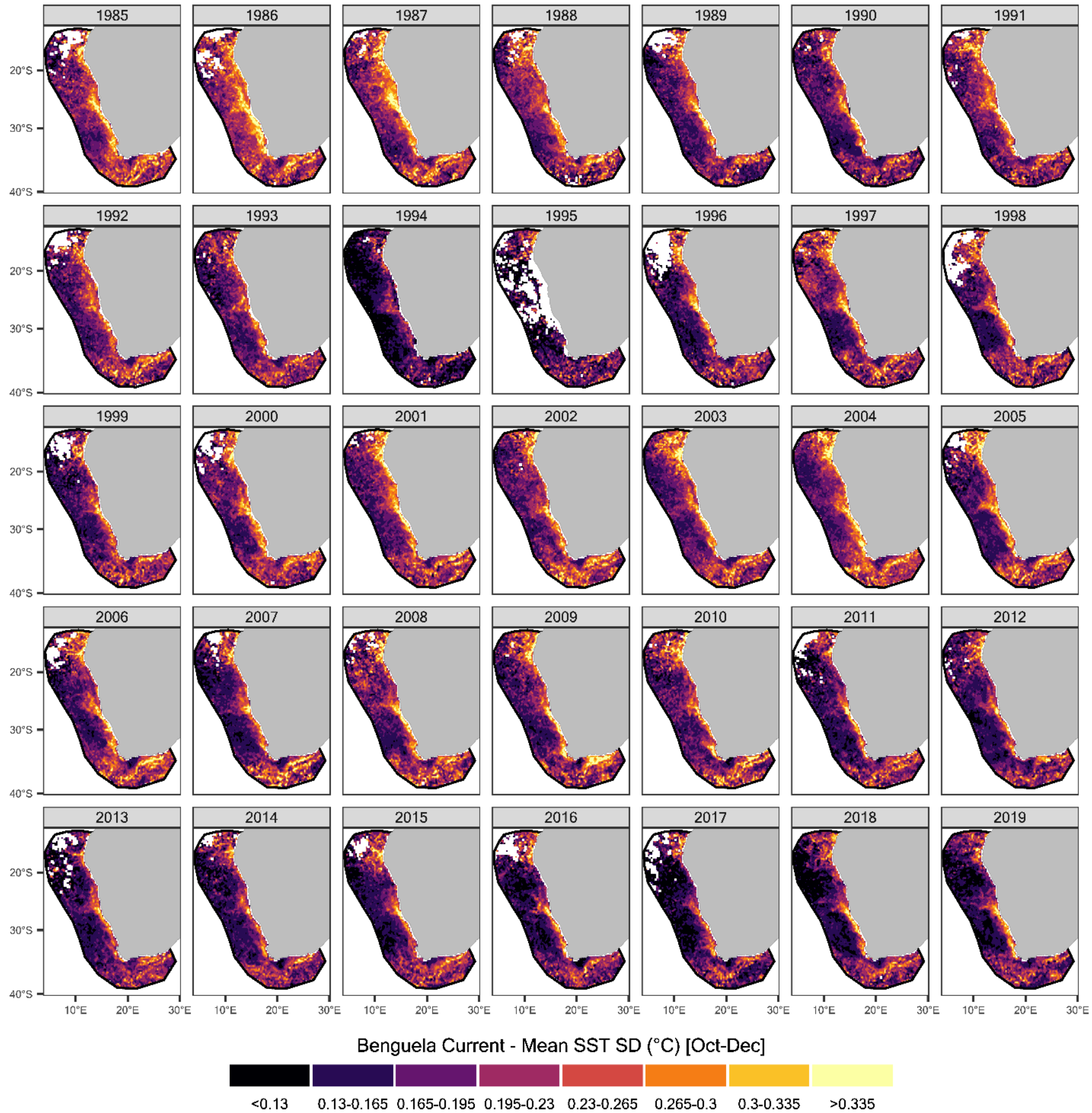

Figure S5. The three-month mean spatial standard deviation (SD) of sea surface temperature (SST) in the Benguela Current spanning 1985-2019.